BBA - General Subjects 1863 (2019) 82–95

Contents lists available at ScienceDirect

BBA - General Subjects

journal homepage: www.elsevier.com/locate/bbagen

Atomistic mechanism of the constitutive activation of PDGFRA via its transmembrane domain

Anton A. Polyansky[a,b,*], Eduard V. Bocharov[a,c,d], Amélie I. Velghe[e], Andrey S. Kuznetsov[a,c,f], Olga V. Bocharova[a,c], Anatoly S. Urban[a,c], Alexander S. Arseniev[a,c], Bojan Zagrovic[b], Jean-Baptiste Demoulin[e,**], Roman G. Efremov[a,c,f]

[a] MM Shemyakin and Yu A Ovchinnikov Institute of Bioorganic Chemistry, Russian Academy of Sciences, Miklukho-Maklaya, 16/10, 117997 Moscow, Russia
[b] Department of Structural and Computational Biology, Max F. Perutz Laboratories, University of Vienna, Campus Vienna Biocenter 5, A-1030 Vienna, Austria
[c] Moscow Institute of Physics and Technology (State University), Institutskiy Pereulok 9, Dolgoprudny, Moscow region 141700, Russia
[d] National Research Centre "Kurchatov Institute", Akad. Kurchatova pl. 1, Moscow 123182, Russia
[e] de Duve Institute, Université catholique de Louvain, Avenue Hippocrate 75, 1200 Brussels, Belgium
[f] Higher School of Economics, Myasnitskaya 20, 101000 Moscow, Russia

ARTICLE INFO

Keywords:
Receptor tyrosine kinases
Oncogenic mutations
Dimerization of transmembrane domains
Signal transduction
Molecular dynamics
NMR

ABSTRACT

Single-point mutations in the transmembrane (TM) region of receptor tyrosine kinases (RTKs) can lead to abnormal ligand-independent activation. We use a combination of computational modeling, NMR spectroscopy and cell experiments to analyze in detail the mechanism of how TM domains contribute to the activation of wild-type (WT) PDGFRA and its oncogenic V536E mutant. Using a computational framework, we scan all positions in PDGFRA TM helix for identification of potential functional mutations for the WT and the mutant and reveal the relationship between the receptor activity and TM dimerization via different interfaces. This strategy also allows us design a novel activating mutation in the WT (I537D) and a compensatory mutation in the V536E background eliminating its constitutive activity (S541G). We show both computationally and experimentally that single-point mutations in the TM region reshape the TM dimer ensemble and delineate the structural and dynamic determinants of spontaneous activation of PDGFRA via its TM domain. Our atomistic picture of the coupling between TM dimerization and PDGFRA activation corroborates the data obtained for other RTKs and provides a foundation for developing novel modulators of the pathological activity of PDGFRA.

1. Introduction

The transmembrane (TM) domains of receptor tyrosine kinases (RTKs), single-pass membrane proteins in charge of regulating cell division and growth, have been shown to play a crucial role in the dimerization and activation of these receptors. Importantly, it is known that even single-point mutations in RTK TM domains may cause a number of severe disorders including human inherited diseases and cancer [1,2]. Despite extensive experimental efforts, however, the atomistic mechanism behind such effects is far from being fully understood.

In order to understand activation of RTKs by single-point mutations at a detailed molecular level, we present here a systematic study of the structural, dynamic, thermodynamic and functional effects of mutations in the TM domain of platelet-derived growth factor receptor alpha (PDGFRA), an RTK with essential roles in embryo development [3,4]. Importantly, PDGFRA is aberrantly activated in many neoplasms such as glioblastoma, gastrointestinal stromal tumors and chronic eosinophilic leukemia. Oncogenic activation of PDGFRA is caused by point mutations, gene amplification, gene fusion or autocrine production of the ligand [5] [4]. Indeed, we have previously shown that V536E substitution in the PDGFRA TM domain is sufficient to constitutively activate the receptor [6]. This mutation was identified in glioblastoma patients in two independent studies [7,8]. Activation of wild-type PDGF receptors requires dimerization induced by a dimeric ligand and conformational changes in the extracellular domain [9], but the exact mechanism of how PDGFRA transmits signals across the membrane is not known. It should, however, be added that the juxtamembrane

* Corresponding author at: MM Shemyakin and Yu A Ovchinnikov Institute of Bioorganic Chemistry, Russian Academy of Sciences, Miklukho-Maklaya, 16/10, 117997 Moscow, Russia.
** Corresponding author.
E-mail addresses: anton.polyansky@univie.ac.at (A.A. Polyansky), jean-baptiste.demoulin@uclouvain.be (J.-B. Demoulin).

https://doi.org/10.1016/j.bbagen.2018.09.011
Received 29 June 2018; Received in revised form 12 September 2018; Accepted 16 September 2018
Available online 22 September 2018
0304-4165/ © 2018 Elsevier B.V. All rights reserved.

domain between the TM helix and the kinase domain may also be critical for silencing the receptor in the absence of a ligand [5] [4].

In addition to being motivated by the intrinsic importance of PDGFRA in different physiological and biomedical contexts, we use it here as a model system to understand further the atomistic mechanism of RTK activation by TM domains in general. Previously, we have shown that the conformations of RTK TM domains are fine-tuned by the lipid environment, while pathogenic single-point mutations in those regions induce conformational rearrangements, affect dimerization strength and potentially facilitate spontaneous activation of the receptors in the absence of ligands [10] [11]. Indeed, according to the dominant view of the coupling between TM domain dimerization and RTK activation, a conformational transition from a non-active TM dimeric state (coexisting in a preformed ligand-free receptor dimer) to an active one occurs upon ligand binding. This rearrangement provides an allosteric signal for the formation of an asymmetric dimer of kinase domains with a subsequent phosphorylation event *in trans*. Such a mechanism has been proposed initially for ErbB2 receptor based on modeling of TM dimer conformations [12], while the capability of ErbB2 to form two different TM dimeric structures has further been confirmed by NMR spectroscopy in membrane mimetics [13] [14]. A similar mechanism has been suggested for another ErbB family member, EGFR, based on a combination of mutagenesis, modeling and NMR spectroscopy [15] [16]. A conformational switch between non-active and active TM dimeric states has also been connected to the activation of type I cytokine receptors – thrombopoietin receptor [17] [18] and growth hormone receptor [19] [20]. Such a conformational transition in the TM region is typically associated with the presence of alternative well-defined dimerization motifs in the TM sequence, like in the case of ErbB receptor family. In this regard, PDGFRA represents a challenging model system since no obvious dimerization motifs (e.g. glycophorin-like motifs) can be found in its TM sequence (Fig. 1a). Moreover, no structural information exists for this receptor, but only its homolog – PDGFRB (48% of identity in the TM region, Fig. 1a), for which the TM dimeric conformation has been obtained by NMR [21] and whose ligand-bound full-length organization has recently been probed by negative-stain electron microscopy [22].

Here, we use a combination of computational modeling and experiment in order to elucidate the contribution of TM domains to PDGFRA activation in normal and pathological states. First, we scan all possible functional amino-acid substitutions in the TM helix of the WT PDGFRA and its V536E mutant using the PREDDIMER [23] based framework, in which mutational effects are related to the packing quality of different reference states. Second, we experimentally test candidate mutations, while controlling for specificity of predicted mutations by "glutamate-screening" and mutagenesis in a constitutively active non-TM mutant background. This is followed by the calculations of association free energies of WT and mutant TM dimers and a low-resolution NMR analysis of the character of TM dimerization for WT, V536E and compensatory V536E/S541G mutant. Finally, we use all-atom molecular dynamics (MD) simulations in order to identify structural and dynamical signatures of active and non-active TM dimer conformations for the WT and the V536E mutant.

2. Material and methods

2.1. Identification of modulating mutations

To estimate quantitatively the packing quality of PDGFRA TM sequences, we have used a stand-alone version of the PREDDIMER web-server (http://model.nmr.ru/preddimer/), which predicts 3D conformation of a TM dimer based on respective TM sequences and ranks the predicted states according to an empirical scoring function (Fscor) [23]. Here, this approach was used to scan the effect of single point mutations in WT and V536E TM sequences (residues 525–549, Fig. 1a, underlined) on helix packing in different dimeric states. We have probed 18 types of amino-acid substitution (excluding the helix breaker Pro and the covalent-dimerization promoting Cys) and each of the 25 and 24 positions of WT and V536E PDGFRA TM sequences, respectively. For each of those sequences, we have predicted top-scoring left-handed (among 3 possible helix-helix crossing angles (Ω): 40°, 45°, and 50°), right-handed (−40°, −45°, −50°) and near parallel conformations (−5°, 0°, 5°) for a total of approx. 8×10^3 different dimer conformations under consideration. Mutation effect was estimated according to MUTSCORE value:

$$MUTSCORE_i = RMS^{Fscor}(i, WT) - RMS^{Fscor}(i, MUT) - \{\sigma_i^{Fscor} - \sigma_{ref}^{Fscor}\},$$

where $RMS^{Fscor}(i, WT)$ is the root-mean-square deviation of Fscor values of dimer conformations for i substituted variant from the reference WT ensemble; $RMS^{Fscor}(i, MUT)$ is the root-mean-square deviation from the reference V536E ensemble; σ_i^{Fscor} – standard deviation of Fscor values in i-mutant ensemble; σ_{ref}^{Fscor} – standard deviation of Fscor values in the *reference* dimer ensemble (WT or V536E). If an i^{th} substituted variant is more similar when it comes to packing to V536E than to WT, ΔRMS^{Fscor} term will have a positive value and if this substitution also decreases σ_i^{Fscor} of a dimer ensemble (makes it more redundant in terms of Fscor) as compared to WT then $-\Delta\sigma^{Fscor}$ also will add a positive value to $MUTSCORE_i$. Thus, high $MUTSCORE_i$ values in such a case indicate a similarity between ensembles of the i^{th} substituted variant and the V536E mutant and suggest a potential activating effect of the i^{th} substitution. For analysis of mutations in V536E, we have used $-MUTSCORE_i$ values.

2.2. Modeling of 3D conformations for TM dimers

For each of the considered PDGFRA variants (WT, I537G, L534G, I537D, V536E, V536/A529I, V536/I540D, V536/S541G), we have predicted ensembles of their dimeric conformations using the PREDDIMER web-server [23] in the Ω angles range of (−60°:60°) and have selected among them three top-scoring conformations for further molecular dynamics simulations (see Table S1 for details). Glutamic and aspartic acids have always been considered in the protonated state (neutral).

Next, we combined different simulation protocols depending on a particular modeling task. To rank the free-energetically different dimer configurations, we used a previously optimized protocol for united-atom GROMOS force field and flexible 1,2-dimyristoyl-sn-glycero-3-phosphocholine (DMPC) bilayer, which is closer to the membrane mimicking media used in NMR. To study the dynamics of individual states at the best possible resolution, we used an all-atom Amber force field and switched to 1-palmitoyl-2-oleoyl-sn-glycero-3-phosphocholine (POPC) as it approximates the plasma membrane more realistically.

2.3. Calculation of dimerization free energy from molecular dynamics (MD) simulations

All MD simulations were performed using the GROMACS 4.5 package [24], the united atom GROMOS96 force field (*43a2x* parameter set) and SPC water model [25]. Simulations were carried out using an integration step of 2 fs and imposed 3D periodic boundary conditions. A twin-range (10/12 Å) spherical cutoff function was used to truncate van der Waals interactions. Electrostatic interactions were treated using the particle-mesh Ewald summation (real space cutoff 10 Å and 1.2 Å grid with fourth-order spline interpolation). MD simulations were carried out in an isothermal-isobaric (NPT) ensemble with a semi-isotropic pressure of 1 bar and a constant temperature of 315 K. The pressure and temperature were controlled using a V-rescale thermostat [26] and a Berendsen barostat [27] with 1.0 and 0.1 ps relaxation parameters, respectively, and a compressibility of 4.5×10^{-5} bar^{-1} for the barostat. Protein, lipids and water molecules were coupled separately. Bond lengths were constrained using LINCS

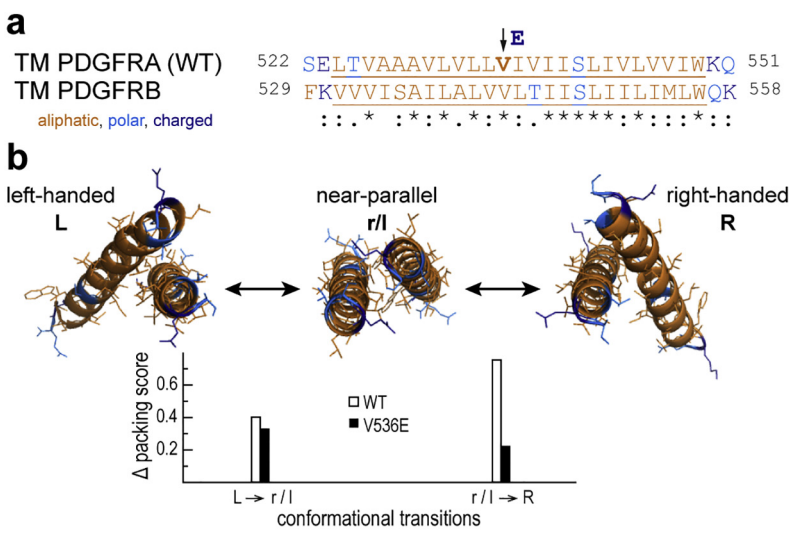

c

	A	D	E	F	G	H	I	K	L	M	N	Q	R	S	T	V	W	Y
L 525		0.2				0.3					0.3							
T 526			0.3															
V 527							0.1											
A 528			0.3						0.2					0.6				
A 529		0.3			0.5													
A 530			0.3											0.1	0.2			
V 531			0.2		0.3							0.4	0.3					0.3
L 532		0.6	0.5		0.6	0.3				0.2	0.5	0.4	0.4	0.3	0.1			
V 533	0.1	0.5	0.6		0.6					0.3	0.5	0.6	0.3	0.6				
L 534		0.6	0.1		0.3							0.2	0.5	0.2				
L 535				0.1	0.4						0.2	0.2			0.3	0.2	0.3	
V 536		0.6	0.6					0.4			0.3			0.6			0.3	
I 537	0.5	0.7	0.6		0.5			0.1		0.4	0.4		0.2	0.7	0.1	0.3		
V 538	0.5	0.3	0.2		0.6						0.5			0.6	0.5	0.2		
I 539	0.3	0.3	0.4		0.6			0.3	0.3				0.6	0.6			0.5	
I 540		0.7	0.3		0.7	0.2					0.5		0.6	0.2	0.2	0.1		
S 541																		
L 542			0.3		0.6		0.1			0.1						0.1		0.4
I 543	0.1	0.4	0.2		0.1	0.4											0.3	0.3
V 544	0.1				0.2								0.5					
L 545		0.3	0.1								0.1	0.2		0.3	0.5	0.2		
V 546	0.1				0.1			0.1			0.2			0.2	0.6			
V 547											0.1							
I 548				0.1														
W 549								0.2										

	A	D	E	F	G	H	I	K	L	M	N	Q	R	S	T	V	W	Y
L 525	0.2							0.3					0.2					
T 526	0.3	0.3		0.4					0.4	0.6						0.3		0.6
V 527	0.5				0.3					0.4	0.2	0.4						
A 528				0.2			0.1	0.6	0.4						0.2	0.4		
A 529		0.5				0.4	0.2	0.4					0.3		0.2	0.3	0.2	0.2
A 530				0.1	0.2		0.5		0.4	0.4	0.4				0.1			
V 531																		
L 532				0.1			0.2										0.4	0.2
V 533				0.1					0.2								0.2	0.7
L 534							0.2		0.2									0.5
L 535		0.7						0.5						0.3				
I 537									0.5						0.1			
V 538			0.5	0.2				0.2	0.2			0.2	0.2	0.2				
I 539																0.4		
I 540				0.2						0.2						0.1	0.4	0.6
S 541			0.2		0.5		0.4				0.2	0.1			0.3	0.2		0.2
L 542								0.3			0.2	0.6						
I 543								0.3				0.3	0.2					
V 544								0.3	0.2	0.3	0.4	0.5						
L 545							0.2										0.4	0.5
V 546	0.1			0.3			0.4	0.4			0.5		0.3	0.4				0.6
V 547	0.5										0.1		0.3				0.2	
I 548					0.1				0.2					0.2				
W 549	0.2				0.3						0.4			0.4	0.3	0.2		

Fig. 1. Computational design of activating mutations in WT and compensatory mutations in V536E. a) Sequence alignment for TM domains (underlined) of PDGFRA and PDGFRB. b) A schematic illustration of the modeling framework. A bar chart depicts absolute changes in the dimer packing score of WT (open bars) and V536E (black bars) for a transition from the left-handed to the near-parallel conformation (*L* - > *r/l*), and from the near-parallel conformation to the right-handed one (*r/l* - > *R*). c) Mutagenesis roadmaps for WT and V536E. Top scoring values in each panel are highlighted in green. MUTSCORE values below 0.1 are not shown for clarity. The residues forming the dimerization interface I (see Fig. 3c for details) are highlighted in bold.

[28].

The initial configurations of the simulated systems were obtained by inserting a dimeric conformation of TM helices with flanking N- and C-terminal polar residues (residues 523–551, Fig. 1a) into a pre-equilibrated lipid bilayer comprised of 128 DMPC molecules using the *genbox* utility from the GROMACS package. The latter procedure leads to the removal of a number of lipid molecules (10 − 20) to form an appropriate pore. Water molecules were added to the simulation box, and waters placed in the bilayer interior were removed. The systems, thus prepared, were equilibrated by energy relaxation via 50000 iterations of the steepest descent minimization followed by heating from 5 K to 315 K during a 50 ps MD run and a 5 ns MD run at 315 K with fixed *x*- and *y*-positions (the bilayer is oriented orthogonal to the *z*-axis) of the peptide atoms to compensate for the bilayer distortion. Finally, production MD runs of 50 ns were carried out for each system.

Potential of mean force (PMF) profiles for each dimer were calculated as a function of inter-helical distance. The distance between the centers of mass was considered as a reaction coordinate *r*. In total, 32 windows were taken for the umbrella sampling with *r* varying from 7.0 to 22.5 Å. A set of reference structures was obtained by translating monomers in the membrane plane along the line connecting their centers of mass. The initial structure for each window was generated using a 50 ns MD equilibration (with the same protocol as mentioned before), where positions of the monomers were fitted to the reference structure. The 50 ns production MD runs were carried out in each window with a harmonic force constant of 10 kJ mol^{-1} $Å^{-2}$. The first 5 ns of each MD trajectory were designated as final equilibration and were not included in the subsequent analysis. The total PMF profile of the dimer association was calculated by integrating the mean force $< F(r) >$, where *F(r)* is the projection of the total force on *r* vector [29]. Error estimation for each run was done by dividing the MD trace into 5 parts, which were used for an independent generation of the profiles.

2.4. All-atom long-term MD simulations

MD simulations were performed using GROMACS 4.5 package [24] and Amber99SB-ILDN force-field [30] with lipid parameters (Slipids) [31] and TIP3P water model [32]. The initial configurations of the simulated systems were obtained by inserting dimer conformation into a pre-equilibrated lipid bilayer comprised of 200 POPC molecules using the *genbox* utility from the GROMACS package. After this step was complete, the system was energy minimized and subjected to an MD equilibration over 30000 steps using a 0.5 fs time step and 250000 steps using a 1 fs time step. Finally, production runs of 200 ns were carried out for all systems using a 2 fs time step. A twin-range (10/14 Å) spherical cut-off function was used to truncate van der Waals interactions. Electrostatic interactions were treated using the particle-mesh Ewald summation (real space cutoff 10 and 1.2 Å grid with fourth-order spline interpolation). MD simulations were carried out using 3D periodic boundary conditions in the isothermal − isobaric (NPT) ensemble with an isotropic pressure of 1.013 bar and a constant temperature of 310 K. The pressure and temperature were controlled using Nose-Hoover thermostat [33] and a Parrinello-Rahman barostat [34] with 0.5 and 10 ps relaxation parameters, respectively, and a compressibility of 4.5×10^{-5} bar^{-1} for the barostat. Protein, lipids and water molecules were coupled separately. Bond lengths were constrained using LINCS [28].

2.5. MD analysis

All analyses were done using utilities from the GROMACS 4.5 package [24] and Linux scripts specially written for this purpose. Particularly, the following structural parameters of a dimer were calculated using GROMACS utilities: root-mean-square deviation from the starting configuration and a reference MD trajectory (RMSD, *g_rms*), a cumulative rotation angle of helices with respect to each other (*g_helixorient*), distances between terminal atoms, W549 and K550 residues (*g_dist*). An average number of van-der-Waals lipid contacts for each protein residue was calculated using *g_dist* with an applied 3.5 Å cut-off for any interatomic distances between the two moieties. The same protocol was used for calculations of helix-helix interface contacts within a dimer. Evolution of the crossing angle between TM helices (Ω) during MD was calculated with the utilities specially written for this purpose. The conformational entropy of each individual lipid molecule was calculated using quasi-harmonic (QH) approach as described elsewhere [35]. The characteristic dynamics of different dimer states were extracted using calculations of eigenvectors from mass-weighted variance-covariance matrices obtained for MD distribution of x-,y-,z-atomic degrees of freedom (*g-covar*). Scalar products between the first eigenvector components corresponding to Cα-atoms of TM helices were calculated. For visualization of the TM dimer dynamics, conformations corresponding to the extremes along the first eigenvectors as well as 8 intermediate states were extracted from MD trajectories (*g_anaeig*). All structures were visualized using Pymol [36].

2.6. PDGFRA constitutive activation in vivo

Experiments were performed essentially as described [6] [37]. PDGFRA mutants were generated using the Quickchange mutagenesis kit (Stratagene) and fully sequenced. Porcine aortic endothelial (PAE) cells were transfected using Turbofect (Life Technologies) with the indicated PDGFRA mutant together with a luciferase reported gene controlled by STAT transcription factors (GRR) and a constitutive β-galactosidase reporter. The ratio between the luciferase and the β-galactosidase activities was calculated for each condition and normalized to the control (vector transfected cells). PDGFRA mutants were stably transfected in Ba/F3 cells. Cells were selected in the presence of G418 and IL-3 and sorted by flow cytometry. Cell proliferation was assessed in the absence of IL-3 (control) or in the presence of PDGF-BB for 24 h, using a tritiated thymidine incorporation assay. Cells stimulated with IL-3 were proliferated to the same extent (data not shown). For Western blot experiments, transfected Ba/F3 cells were washed and cell lysates were analyzed using anti-phospho-Y694-STAT5, anti-STAT5, anti-phospho-S473-AKT or anti-AKT (Cell Signaling Technologies).

2.7. Expression and purification of WT and mutant PDGFRA TM fragments for NMR experiments

The plasmid constructs were based on the pGEMEX-1 vector (Promega). PDGFRA gene fragment was amplified by PCR with flanking primers. A 6 His tag followed by a thrombin site was inserted upstream to the gene. Amplicon was hydrolyzed by *Bam*HI and *Hin*dIII restrictases, the sites of which are located at the 5′- and 3′-ends of the PDGFRA gene, respectively, and then ligated with the vector preliminary subjected to the hydrolysis by the same restrictases. DNA of the selected clones was sequenced within the insertion.

E. coli Rosetta(DE3)/pLysS cells were transformed by the pGEMEX/PDGFRA plasmid and cultivated at 37°C on LB medium for 5 h. Cell culture was diluted into M-5052 autoinduction medium (0.5% glycerol, 0.05% glucose, 0.2% lactose) [38] to the final OD550 equal to 0.1 and incubated for 24 h at 37 °C and 300 rpm.

Cells were centrifuged and pellet lysed in 30 ml of buffer A containing 50 mM Tris-HCl pH 8, 4 M urea, 0.25 M NaCl, 1% lauroylsarcosine, 10 mM β–mercaptoethanol, 0.1 mM phenylmethylsulfonylfluoride. Suspension was sonicated 7 times for 30 s with 5 min pulses in ice bath and centrifuged at 15000 *g* for 20 min. Then the supernatant was applied on Ni-sepharose column preliminary equilibrated with buffer A. Column was washed with buffer B (the same as buffer A, but without urea) for removing urea and buffer C (the same as buffer B but with supplemented with 1% triton X-100) for detergent exchange. Target protein was eluted with buffer E (the same as buffer C but with

250 mM imidazole). Hydrolysis of the hybrid protein was carried out at room temperature; 25 NIH activity units of thrombin per 1 mg of hybrid protein were added and the mixture was incubated for 16–20 h. Protein was precipitated with the Triton X-100 detergent by addition of 15 vol % of the trifluoroethanol thus separating from the thrombin left soluble in the water phase. Precipitate of the target protein and detergent was 2 times washed out of detergent with acetone and solubilized in 0.5% lauroylsarcosine for subtractive chromatography on Ni-high performance sepharose. Unbound protein was reprecipitated with trichloroacetic acid with the subsequent 3-times acetone washing. The precipitate was solubilized in the trifluoroethanol-water mix (2/1 volume ratio) and used for incorporation into the micelles or lyophilized for storage.

2.8. NMR experiments

The ^{15}N-labeled wild-type and mutant PDGFRA TM fragments were incorporated into dodecylphosphocholine (DPC) micelles with an effective detergent/protein molar ratio (D/P) varied from 70 to 1000 at total detergent concentrations varied from 16 to 200 mM. The peptide's powder was first dissolved in 1/1 (*v*/v) trifluoroethanol-water mixture with addition of DPC, then kept for several minutes in an ultrasound bath and lyophilized. After that, the dried 15 N-labeled samples were dissolved at pH 5.0 in 250 μl of a buffer solution, containing 30 mM Na2HPO4, 15 mM citric acid, 0.15 μM sodium azide, and 5% D_2O. The pH value of 5.0 has been chosen to ensure that the TM ionogenic side chains of mutant PDGFRA TM fragments are protonated and uncharged, allowing peptide penetration through the membrane mimetic particle [39]. In order to ensure uniformity of the micelle size, several freeze–thaw cycles were carried out at each D/P point, followed by sonication until the sample became transparent. The 1H/15N-TROSY NMR spectra [40] were acquired for a detection of an oligomeric state and conformation of the ^{15}N-labeled wild-type and mutant PDGFRA TM fragments in the membrane-mimicking DPC micelles at 40 °C on 600 MHz AVANCE III spectrometer (Bruker BioSpin) equipped with the pulsed-field gradient triple-resonance cryoprobe. Partial signal assignment was made based on the NMR spectra of the selectively labeled PDGFRA WT fragments containing 15N-labeled T, K, or W amino acids, as well on the characteristic chemical shifts and signal broadening typical for the residues situated either in TM helix embedded into a micelle or in water-exposed, flexible juxtamembrane regions [41] [16].

3. Results

3.1. Design of activating and compensatory TM mutations in WT and V536E backgrounds

To identify mutations that could modulate dimerization of PDGFRA TM domains, we have used an automated, self-consistent computational framework. Specifically, we have modeled PDGFRA TM dimer conformations using our previously developed PREDDIMER algorithm [23], which reconstructs ensembles of dimeric states based on TM sequences. Previously, we have proposed that PDGFRA TM dimer can form right-handed and left-handed conformations, whereby the latter is similar to the NMR structure of the PDGFRB TM dimer [6]. Here, we perform an in silico scan of each of the 25 and 24 positions in WT and V536E PDGFRA TM sequences, respectively, and analyze the potential effect of all possible single amino-acid substitutions on the dimer geometry and its packing quality. For each sequence, we predict the top-scoring left-handed (*L*), right-handed (*R*) and near parallel conformations (*r/l*), resulting in ca. 8×10^3 different dimer conformations in total. To assess the effect of a given mutation, we define a scoring function (MUTSCORE), which accounts for the change in the heterogeneity of the thus defined dimer ensembles upon mutation and the similarity of packing quality of the resulting conformations with respect to the reference WT and V536E ensembles. In these high-throughput calculations, we use the packing quality as a proxy for the association strength of TM monomers. Note that the heights of the barriers separating different states are also important to consider, but here we focus exclusively on the thermodynamic aspects of the problem at hand i.e. population differences in equilibrium. Thus, our scoring function for mutation screening is based on the idea that conformational ensembles of the TM dimer, whereby multiple states exhibit similar association strengths, may be characterized by facile transitions between them and subsequent *spontaneous* activation, while in the case of the ensembles where the dimer exists in a single predominant state, such transitions would require additional energy input [11]. For example, transitions between *L* and *r/L* dimeric states require a similar level of packing rearrangement in both WT and V536E dimers, while *r/l* to *R* transition requires a larger packing perturbation for the WT than the mutant (Fig. 1b). Altogether, MUTSCORE identifies the position and the type of mutations, which decrease the heterogeneity of the packing quality of mutant conformations with respect to the reference WT ensemble and change in these values towards V536E. Oppositely, compensatory mutations in the V536E background (eliminating its unwanted activation) increase the heterogeneity of the ensemble and make the ranking of states similar to the WT. Note that the scoring function for PDGFRA TM has an absolute maximum value of 0.7 and the values above 0.3 are among the top 10% of the obtained scores in both cases.

Interestingly, the mutations predicted as “activating” for the WT display a defined pattern with regard to the type of amino-acid substitutions and their position in the helix (Fig. 1c). Specifically, most of them affect the prominent aliphatic patch in the middle of the helix (L532-I540), which is responsible for the dimerization via the heptad motif along one possible dimerization interface (termed here “interface I", with positions in Fig. 1c given in bold characters; see also Fig. 3c). Moreover, such mutations involve a limited repertoire of amino acids: Asp, Gly, Ser, Glu, Gln, Arg and Thr, ordered here with respect to the number of possible positions. Similar substitutions in the TM domain are known to be responsible for constitutive activation and pathological effect in different RTK members (ErbB [42] [13] [43] [44], FGFR [41], etc) and typically derive from single nucleotide substitutions in the receptor gene. In contrast to the WT, the mutations predicted as “deactivating” for the V536E display some tendency to be outside of interface I (see below).

3.2. Experimental validation of predicted mutations in cells

To validate the above approach, we have first selected three mutations in the vicinity of V536, that exhibit different values of the scoring function and are among the most likely substitution types (see above): I537D (0.7), I537G (0.5), L534G (0.3), with the scoring values given in the parentheses. We have tested the ability of these mutants to activate PDGFRA signaling by using a luciferase reporter assay that is sensitive to STAT transcription factor activation (Fig. 2a). To confirm these results, we have transfected the mutated receptors into Ba/F3 cells, a classical model system for testing proliferation induced by oncogenes [6] [45] (Fig. 2b). A cell population expressing similar levels of receptors was obtained after selection in the presence of G418 and cell sorting according to receptor expression. Constitutive signaling in these cells was further confirmed by a Western blot analysis using specific antibodies that recognize activated STAT5 and AKT (Fig. 2c, d). Based on these results, we have identified a new activating mutation I537D, which resembles the phenotype of the V536E oncogenic mutant according to all three experiments. Other tested WT mutants (I537G and L534G) display no effect (Fig. 1c, Fig. 2). As an additional control for specificity of the prediction, we performed “glutamate-screening” by introducing Glu at one of the four positions upstream and downstream of V536. Some of these mutants showed a weak activity in the luciferase test, while none of them stimulated Ba/F3 cell proliferation. Also, no evidence of constitutive signaling was found for most of the Glu-mutants by Western blot, except with V536E, used as a positive control,

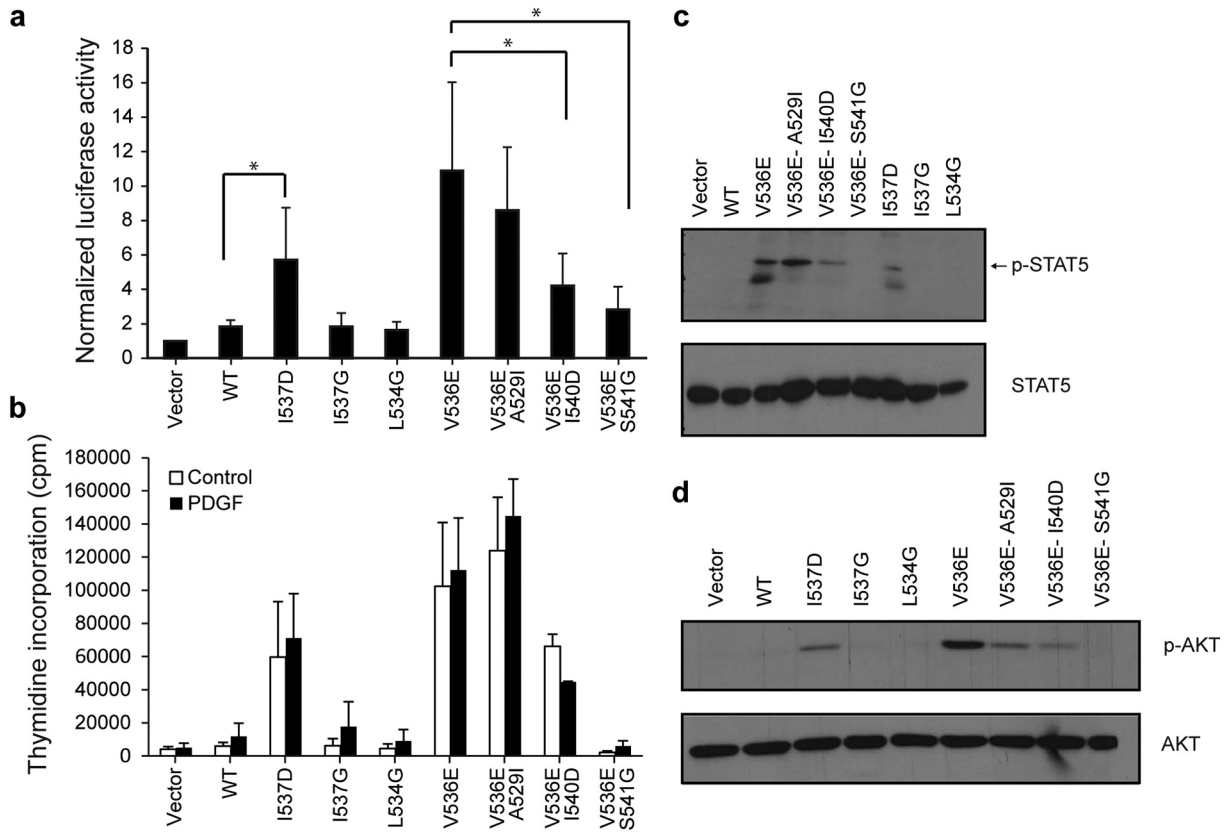

Fig. 2. Validation of the predicted mutations in cell experiments. a) PAE cells were transfected with the indicated PDGFRA mutant together with a luciferase reported gene controlled by STAT transcription factors. The luciferase activity was normalized to the control (vector) condition. The average of three independent experiments is shown. The indicated receptor construct was stably transfected in Ba/F3 cells. b) Cell proliferation was assessed in the absence of IL-3 (control) or in the presence of PDGF-BB for 24 h, using a tritiated thymidine incorporation assay. Cells stimulated with IL-3 proliferated to the same extent (data not shown). Ba/F3 cell lysates were analyzed by Western blot with anti-phospho-STAT5 (c) or anti-phospho-AKT (d) antibodies. The p-STAT5 band is indicated with an arrow.

and V533E, which induces Akt phosphorylation (see Fig. S1 for details) and was also predicted to have an effect in MUTSCORE calculations (Fig. 1c). Altogether, activities of the tested WT mutants correspond well to the predictions of our computational framework, with the most important outcome being the identification of a novel activating mutation I537D.

Using an analogous approach, we next validated our computational predictions in the case of compensatory mutations for V536E. We selected V536E/S541G as a mutation with a relatively high score (0.5) and two mutations with lower scores upstream and downstream of V536, lying on the same face of the TM helix (Fig. 3c): A529I (0.2) and I540D (< 0.2). In the three assays described above, the double mutant V536E/S541G behaved similarly to the WT receptor, indicating that the mutation eliminated constitutive activation (Figs. 1c and Fig. 2). Among other tested substitutions, I540D mutation reduced cell proliferation and signaling significantly, albeit to a lesser extent as compared to S541G. The A529I mutation had no significant impact on the luciferase activity and cell proliferation, but exhibited a decreased ability to activate AKT (Fig. 2). To determine whether S541 works specifically in the V536E background, we introduced the same mutation in the WT and in another oncogenic mutant D842V, which affects the kinase domain activation loop and is recurrently found in gastrointestinal stromal tumors (GIST) [45]. We observed that S541G (predicted to have no activating effect in WT) also reduces the ability of the wild-type receptor to signal and stimulate cell growth, while the relative effect is less dramatic as compared to that in the V536E background (Fig. S2). By contrast, this substitution did not significantly affect the activity of the D842V oncogenic mutation, suggesting that this kinase domain mutation alleviates the requirement for a specific TM domain conformation. We compared the three predicted top-scoring conformations of S541G to those of WT (Fig. S2d). While the *L* and *R* conformations of the two dimers associated via interface I are almost identical, the *r* conformations deviate from each other by 0.2 nm in backbone root-mean-squared deviation (RMSD). Thus, S541G forms a more compact *r* dimer conformation due to tighter helix packing via an alternative dimerization interface ("interface II", Fig. 3c, see below).

3.3. Mutations change association strength at different dimerization interfaces

To analyze in detail the thermodynamics of the dimerization process of the WT and the mutant PDGFRA TM domains via different interfaces, we have employed a previously established modeling framework [10] [11] [46] that combines a relaxation of dimer conformations predicted by PREDDIMER using atomistic MD simulations in an explicit membrane environment (DMPC), followed by the potential of mean force (PMF) calculations (see Methods for details). In particular, for the variants with normal (WT, V536E/S541G, I537G and L534G) and increased activities (V536E, I537D, V536E/A529I, V536E/I540D), we have selected the three top-scoring conformations according to the PREDDIMER packing score in the Ω angle range of (−60°:60°) and obtained their dimerization free energies. This has resulted in approximately 40 μs of total MD statistics. Although DMPC bilayer is much more dynamic and adaptable environment than the cellular membrane, it gives an opportunity to derive free energies for the dimer association along different interfaces that are less affected by particular membrane properties [10], such as hydrophobic thickness [21] and in this sense approximates better the membrane mimetics used in solution

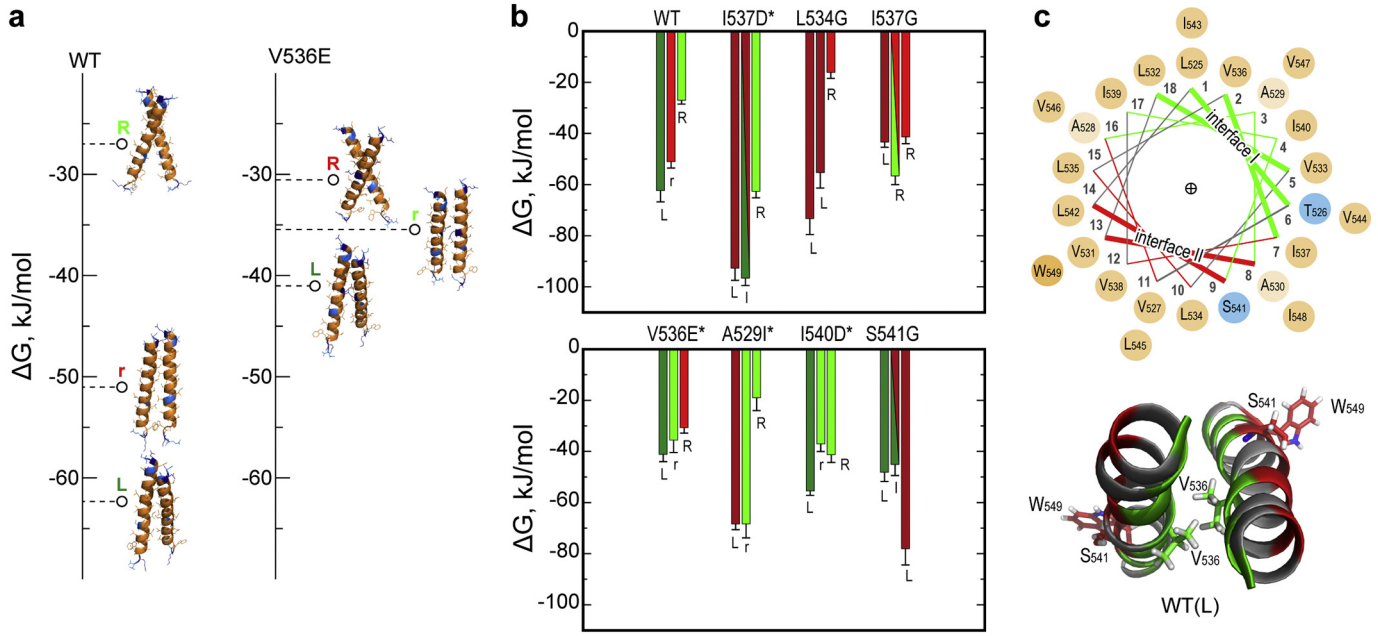

Fig. 3. MD-derived association free energies for the three top-scoring predicted TM dimer conformations of PDGFRA WT and mutants. a) A free-energy diagram for the WT and V536E ensembles. b) Association free energies for all modeled conformations. Constitutively active PDGFRA variants (Fig. 2) are marked with a star. "R" and "L" indicate right-handed and left-handed dimers, respectively. "r" and "l" indicate near-parallel dimer arrangement in the right-handed and left-handed area, respectively. c) The helical-wheel representation of the PDGFRA TM helix and the top view of WT *L* dimer. Alanine, aliphatic and tryptophan residues are shown with orange circles of different shades. Polar serine and threonine residues are shown with blue circles. Green and red lines depict subsets of interface I and interface II helical sides participating in the dimerization, respectively. Helices are shown in cartoon representation, where key residues are shown with sticks and green and red colors correspond to interface I an II, respectively. In panels a) and b) green and red colors correspond to interface I and interface II dimers, where dark and bright tones depict left-handed and right-handed arrangements, respectively. Dimers with mixed I/II interfaces are shown with two colors, respectively.

NMR experiments (see below).

According to the calculated free-energy data (see also Table S1 for details), the lowest energy state of the WT dimer (Fig. 3a) corresponds to the *L* conformation, while *r* and *R* conformations differ from it (11.3 and 35.3 kJ mol^{-1} respectively) and from each other (24.0 kJ mol^{-1}) by substantial free-energy gaps. In contrast, the V536E mutation equalizes different dimer conformations with respect to their association free energies (Fig. 3a) with the substantially reduced free-energy differences for *L* to *r* (5.5 kJ mol^{-1}), *r* to *R* (5.0 kJ mol^{-1}), and *L* to *R* (10.5 kJ mol^{-1}) transitions (for a detailed description of the free-energy ranking of dimer conformations for WT and different mutants see S1 Text). This mutation also in general weakens the association strength of the TM dimer. A similar effect was experimentally observed for the V664E TM mutation in the Neu receptor [47].

We classify the dimer conformations according to their association interfaces using a helical wheel projection of the TM helix (Fig. 3c). Analysis of MD relaxation trajectories for the top-scoring conformations of 8 TM variants shows that most of them form dimers between two well-defined, nearly opposite faces of the helix, which are depicted in green (interface I) and red (interface II), respectively. In the WT, the *L* and *R* dimers associate via interface I, while the *r* dimer associates with interface II (Fig. 3a, c). Interestingly, V536E helices undergo dimerization, where *r* and *R* conformations swap interfaces as compared to the WT dimer. In particular, the V536E *L* and *r* conformations associate via interface I, while the *R* conformation is formed by the opposite sides of helices (interface II). Moreover, their free-energy ranking is prominently different from the WT (Fig. 3b). Thus, spontaneous transition to interface I *R* conformation (green bar) is restricted in WT by a free-energy penalty. In contrast, V536E *r* dimer associating via the interface I is energetically not too distant from the dominant *L* state. For other variants of V536E, we also observe that the presence of the favorable interface I, *R* (or *r*) dimer conformations in the ensemble corresponds to constitutive activation of the receptor (Fig. 3b). The I537D activating mutation in the WT perturbs the dimer ensemble more strongly as compared to the V536E mutation due to the introduction of an additional H-bond between D537 and S541 (Fig. S3), which stabilizes conformations with interface II (*L*) and the mixed I/II ones (*l*). The right-handed I537D dimer with the interface I is the most stable among other tested variants, although it is separated by a significant free energy gap from the left-handed ones. Such a difference between V536E and I537D at the ensemble level can potentially explain the fact that, although the latter mutation mimics activation of the oncogenic one, the level of activation is smaller (Fig. 2). The Gly mutations in the WT also display a common trend in that they stabilize conformations with interfaces where they introduce a glycophorin-like dimerization motif. Namely, these are interface II conformations in L534G (Fig. 3b) and mixed I/II conformations in I537G (Fig. 3b, two-color bar). The L534G and I537G mutants, however, display no favorable dimerization via interface I, which can potentially explain the absence of constitutive activation for these mutants. Finally, the S541G mutation in the V536E background, in addition to restricting the left-to-right transition, also eliminates any favorable conformations with interface I.

3.4. Activating and compensatory mutations directly modulate TM dimerization according to fingerprinting NMR spectra

To probe the direct effect of TM mutations on PDGFRA TM domain dimerization and validate the modeling data, we have acquired $^{1}H/^{15}N$-heteronuclear NMR spectra in membrane-mimicking dodecylphosphocholine (DPC) micelles for three ^{15}N-labeled recombinant fragments corresponding to TM fragments of WT, V536E, and V536E/S541G variants (see Methods for details). While high-resolution NMR data were out of scope of the present study, we have managed to perform partial assignment of the signals from N- and C-terminal peptide residues for the obtained NMR spectra (see Methods for details). These fingerprinting spectra clearly demonstrate that all tested PDGFRA TM fragments adopt mostly a helical conformation having the characteristic dispersion from 7.5 ppm to 9.0 ppm for the ^{1}H-chemical shifts of the

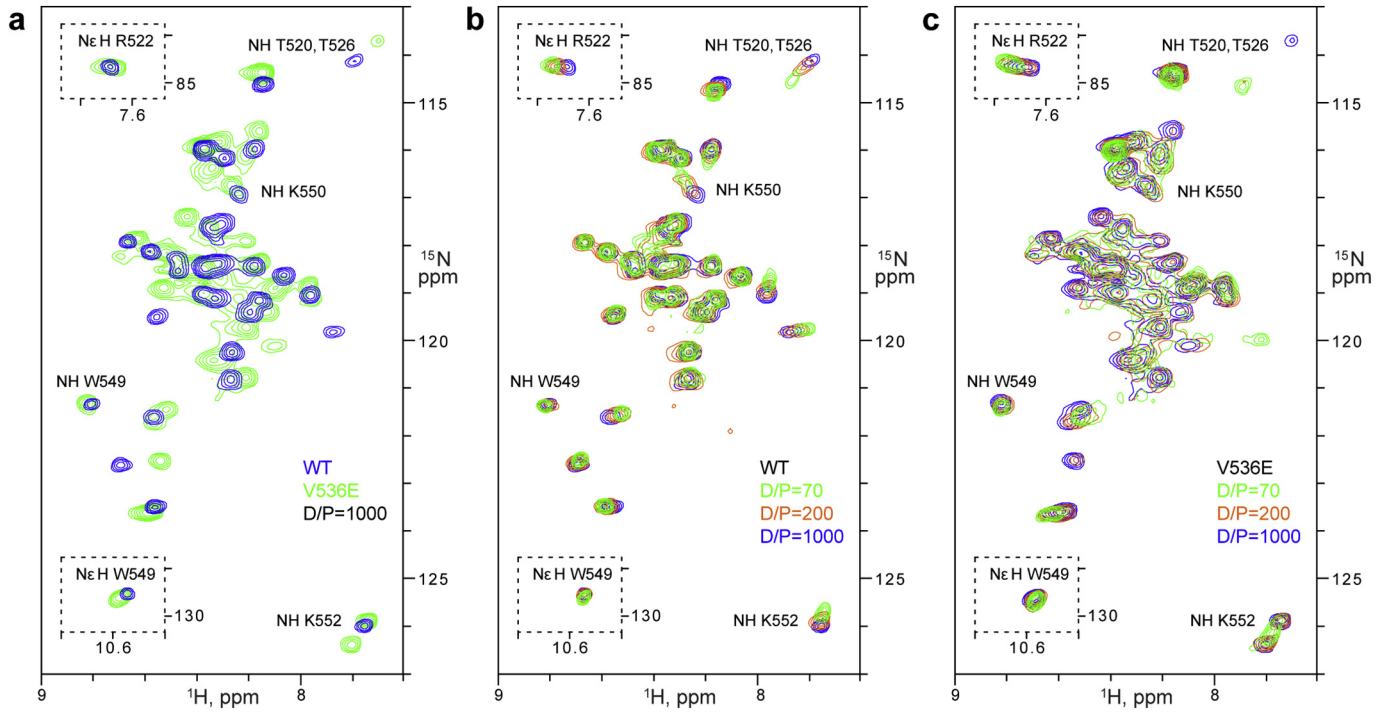

Fig. 4. Oligomerization in vitro. Overlaid $^{1}H/^{15}N$-heteronuclear NMR spectra: a) WT and V536E at detergent/protein (D/P) ratio of 1000; b) WT at different D/P ratios; c) V536E at different D/P ratios.

amide groups (Fig. 4, Fig. S4). Using 3 different detergent-to-peptide ratios (D/P: 1000, 200, and 70), we observe concentration-dependent signal perturbations (doubling, broadening and shifting) in the NMR spectra of the fragments. Thus, $^{1}H/^{15}N$-TROSY NMR spectrum of WT at $D/P = 1000$ mostly resembles monomeric signals, while decreasing the D/P ratio leads to broadening and shifting of the NH cross-peaks due to a perturbation of the WT TM fragment structure. Such stepwise perturbation can be caused by increased self-association of the TM helices in the micelles saturated by the peptide (Fig. 4b), as is typical for weakly dimerized/oligomerized TM domains of different proteins [41] [16,48]. Low dimerization of WT at high D/P ratio is also in line with SDS-PAGE experiments, where the WT TM fragment exists preferably in a monomeric state (Fig. S4a). On the basis of these data, we conclude that the association of the WT TM fragments at a lower D/P ratio populates a dimeric state, whereby the NMR signals coming from both the N-terminal part of the peptide (NεH R522, NH T520 and T526) and the C-terminal part (NεH W549, NH W549, NH K550, NH K552) appear to be affected by self-association that may indicate near-parallel arrangement of the WT dimer corresponding to the predicted *r* conformation (Fig. 3a). It is interesting that in this conformation W549 and K550 can form a cation-pi interaction pair (see below) that can be related to wide-range shifts of NH K550 cross-peaks upon titration.

According to the fingerprinting NMR spectra and SDS-PAGE (Fig. 4a, c, Fig. S4a), the V536E mutation strongly affects conformational behavior and self-association of TM helices. First, even at the D/P ratio of 1000, the $^{1}H/^{15}N$-TROSY NMR spectrum of the V536E mutant displays a tendency to strongly self-associate as can be concluded from the comparison of its spectrum with that of the WT. Particularly, self-association leads to broadening and doubling of most of the NH cross-peaks. The character of the V536E spectra also suggests slower conformational exchange as compared to the WT, which is also illustrated by the presence of a stable V536E dimer band in the SDS-PAGE experiment (Fig. S4). For the assigned signals, we observe the effect in both N- (NεH R522, NH T520 and T526) and C-terminal parts (NεH and NH W549, NH K550, NH K552). While NεH and NH W549 peaks become broader as compared to the WT, the signals of NH K550, already at the D/P ratio of 1000, are located near the position of those in the WT spectra at low D/P ratios (Fig. 4a) and do not display significant changes upon decreasing the D/P ratio (Fig. 4c). At the same time, the signals of NH K552 are split into two distinct peaks indicating the presence of at least two discrete states in the ensemble (Fig. 4a, c). The occupancy of the dimeric state is increased from 40% at the D/P ratio of 1000 to 56% at the D/P ratio of 200. Further, we speculate that the spectrum of V536E at the high D/P ratio corresponds not only to monomer-dimer transitions, but also captures the presence of another dimeric state with an alternative interface. Decreasing the D/P ratio leads to an even more prominent oligomerization and populates an alternative state, which is reflected in the diffuse shape of the spectra (Fig. 4c). Importantly, at the D/P ratio of 70, two independent peaks corresponding to NH K552 merge, potentially indicating the presence of higher oligomers (e.g. tetramers, see below) comprising different dimer conformations and/or the appearance in the ensemble of an additional dimeric state. We should mention that in contrast to the WT, both mutants display a strong tendency to oligomerize even in SDS-PAGE, where we detect bands not only for dimers, but also for oligomers of different sizes (Fig. S4a). In particular, a compensatory mutation S541G seems to potentiate the oligomerization of V536E, which results in the noisy character of its spectrum even at the D/P ratio of 1000 (Fig. S4c, d). Although it is difficult to interpret the spectra of the double mutant without additional information, it is clear that the S541G mutation almost completely depletes the additional NH K522 signal at 8.2/126.5 ppm for the ^{1}H-/^{15}N-chemical shifts for all tested D/P ratios and also narrows the signals of NεH and NH W549, and NH K550 as compared to V536E (Fig. S4c, d, Fig. 4c). For the latter one, we attribute these signals at the high D/P ratio to the *R* dimer, where helices undergo dimerization via interface II of the C-terminal part of the peptide (Fig. 3c) engaging S541 and W549 into inter-helical contacts. An alternative dimer state for V536E at the high D/P ratio seems to be related to dimerization via the interface I. Particularly, the wider range of shifts observed in the V536E for NH T526 peaks as compared to the WT suggests a potential contribution of this interface I residue to the dimerization. At the D/P ratio of 70, the two alternative dimers can

arrange into higher oligomers, e.g. a putative tetramer, where the *R* dimeric conformation (interface II) represents a core, while additional helices are bound to this dimer via interface I engaging E536 for inter-helical contacts, resulting in the formation of two additional *L* dimers (Fig. S4b).

3.5. V536E mutation introduces a hinge and slows down TM dimer dynamics

To investigate the characteristic dynamics of individual dimeric states that could contribute to the allosteric signal transduction upon PDGFRA activation in the case of the WT and the V536E mutant, we have performed extensive all-atom MD simulations of the respective three top-scoring dimer conformations in a POPC bilayer (see Methods for the details). In contrast to the rather fluid DMPC used for relaxation and free energy calculations of TM dimers (see above), POPC is supposed to mimic better the cell membrane. According to the MD data, all WT dimer conformations are found to be relatively more dynamic and structurally heterogeneous as compared to V536E. Thus, backbone RMSD values (Fig. S5a, b) of WT states exceed 0.3 nm in the course of simulations, while for both the *L* and *R* V536E dimers the deviations remain below 0.25 nm and only the near-parallel conformation deviates more significantly from the start. Such an effect has a direct structural explanation: E536 (protonated in MD simulations), when residing on the dimer interface (interface I), can form very stable intermolecular van-der-Waals contacts with neighboring V533 and I540 as well as hydrogen bonds with a Glu from another helix (Fig. S6). These additional contacts, which are absent in the WT, constrain dynamics in the mutant dimer. For the near-parallel models of the WT and the V536E mutant (initially right-handed, hereinafter *r/l*), we observe a re-arrangement to the left-handed conformations (the Ω angle time series, Fig. S5c, d). Whereas for the V536E *r/l* conformation these rearrangements seem to be rather reversible with multiple forward-and-back, right-to-left transitions, this transition displays an irreversible character in the case of the WT. The *r/l* conformation of V536E becomes similar to the *L* states during MD (Fig. S7a, b), corroborating the above results showing the redundancy of the V536E dimeric ensemble and small energy gaps between the *r/l* and the *L* states. In contrast to the mutant, the near-parallel conformation of the WT transits to the left-handed state distinct from the *L* dimer (Fig. S7a, b). The observed dynamics of the dimer is modulated by its interaction with the POPC lipid environment, where the exposed dimer surface and geometry predefine the character of protein-lipid interactions. The total MD-averaged number of such lipids varies between the WT dimer states as follows: 16.1, 13.7, and 18.5 molecules for the *L*, *r/l* and *R* conformations, respectively (Fig. S8a). For the mutant dimer, these values are more similar: 15.5, 15.6, and 16.3 molecules, respectively. Interestingly, we observe that polar residues exposed to the lipid matrix (particularly S541) form the most prominent lipid interaction sites (Fig. S8a). From the entropic point of view, arresting of lipids and slowing down of their dynamics by a TM dimer should have an unfavorable thermodynamic effect similar to the hydrophobic effect in water that can be quantified using the calculation of quasi-harmonic (QH) conformational entropy for the lipid molecules (see Methods). In contrast to the mutant, where both of the interface I conformations have a similar entropic effect on lipids, the WT *L* and *R* conformations are prominently different with regards to this parameter (Fig. S8b). The latter WT dimer displays the strongest unfavorable entropic effect among the other states.

3.6. Displacement of C-termini in the TM dimer is constrained by the "cation-pi lock"

Internal dimer dynamics and geometry affect the mutual position of its N- and C-termini (for details see S2 text). Particularly, the dynamics of the C-termini in the TM PDGFRA dimer is shaped by the interaction between the C-terminal residues, e.g. W549 and K550 (Fig. 5a). The latter ones are conserved in different PDGFRs (e.g., in PDGFRB, where K swaps its position with the neighboring Q, Fig. 5b) and can potentially form stable intermolecular cation-pi interactions in the low-dielectric membrane environment [49] [50]. The possibility to form such cation-pi pairs depends on the dimerization interface: in both WT and V536E, only dimers associated via the interface II are able to form short-distance intermolecular pairs between the aforementioned residues (Fig. 5a). Thus, the average MD distances for the two Lys-Trp pairs in the WT *r/l* conformation are 0.66 ± 0.12 nm and 0.72 ± 0.32. Similarly, such interactions are enabled in the V536E *R* conformations, where the corresponding distances are 0.65 ± 0.15 and 1.14 ± 0.14 nm, respectively. Although cation-pi interactions are weaker in the mutant dimer, in both cases the assembly of such a "Lys-Trp lock" for the interface II results in constrained dynamics of the C-termini. Interestingly, neighboring aromatic and basic residues in the C-terminal part of the TM region can also be found in a number of RTKs from the same group of the human "kinome" [51] (Fig. 5b). Such pairs (e.g. Lys/Trp and Lys/Tyr) are particularly enriched in the RTK type III subfamily (also known as PDGF receptor family) that may indicate their functional importance for constraining some particular TM dimer conformations via the cation-pi lock.

3.7. V536E mutation reshapes the dynamic modes of the TM dimer

We have analyzed the dominant dynamics of different dimeric states using calculations of the first and the second eigenvectors of mass-weighted MD-derived variance-covariance matrices [52] and have extracted in this way information about the TM dimer motion in the subterahertz frequency range, corresponding to picosecond collective dynamics of lipid chains [53]. The obtained correlation maps for Cα-atom components of the first eigenvector capture a unique pattern of concerted motions within the dimer (Fig. 5c, d, Fig. S10). For example, we observe large amplitude motions along the first eigenvector in all states for the WT (Fig. S10), where periodic intensity patterns (correlated/anticorrelated motions with periodicity of approx. 4 residues) correspond to a rotation of the helices (see also Fig. S9 and S3 Text). Note that rotation of TM helices inside the lipid bilayer is generally restrained by the environment and, to be sampled at a certain level of completeness, would require a much longer simulation, going even beyond the microsecond range (see e.g. [54]). Here, we observe just partial and rather reversible rotations of helices which do not lead to substantial dimer rearrangement and switch between dimerization interfaces, and should be considered as "breathing" of a given dimer conformation. Apart from just the rotation of the helices, the TM dimers can exhibit a mixture of different types of motion. For instance, for the WT *r/l* dimer, where we detect a transition between right- and left-handed configurations (Fig. S5c) in addition to the rotation of helices, the "butterfly" pattern in scalar-product maps points to a scissor-like movement of the helices (Fig. S10). Surprisingly, the characteristic dynamics of the mutant dimer seems to be prominently different from that of the WT. Thus, mutant dimeric states demonstrate a less-correlated character of large-amplitude motions. Except for the *R* conformation, we do not observe any prominent rotation signatures for other mutant dimer conformations (Fig. S10, Fig. S9). The difference in dynamic patterns is particularly remarkable for similar interface WT (*R*) and mutant dimer conformations (*r/l*). In the WT dimer, the helices rotate with respect to each other in a gear-like manner (Fig. 5c, Movies S1, S2) corresponding to a large-amplitude movement of the dimer C-termini and transitions of the dimer through an asymmetric arrangement. In the case of the mutant, the dynamic mode is a mixture of scissor-like movements with respect to the central hinge (E536-E536) and helices bending in the C-terminal part (Fig. 5d, Movies S3, S4), while the helices seem to be less synchronized in the central part as compared to the WT.

To understand how characteristic dynamics differs in the known active and non-active TM dimer states, we have also performed the

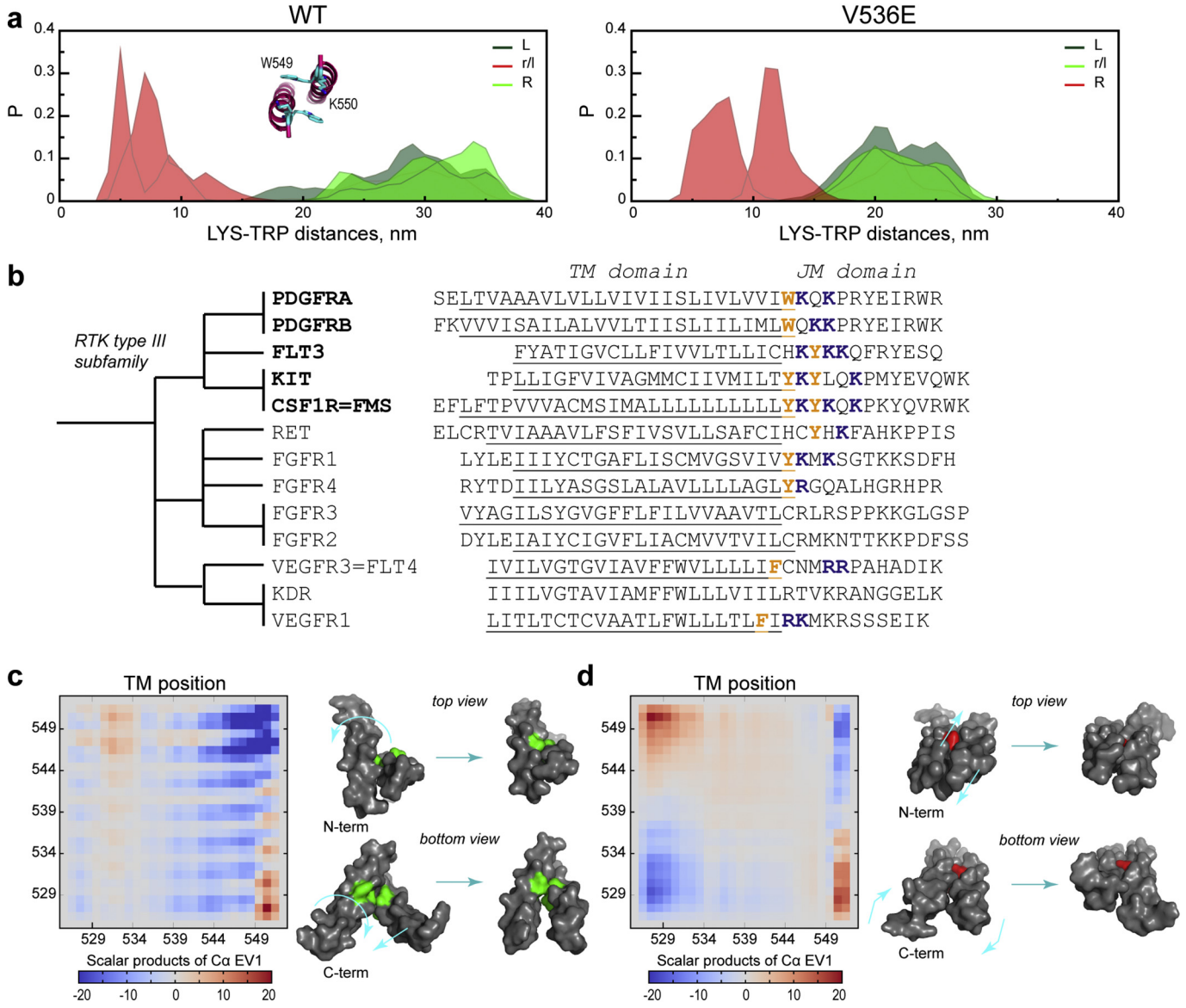

Fig. 5. Dynamics of WT and V536E TM dimers in POPC membrane. a) Distributions of W549-K550 distances in different dimer conformations. Colors correspond to dimerization interfaces (for details, see the caption for Fig. 3). b) Alignment of TM + juxtamembrane sequences for RTKs from the same group [51]. The members of RTK type III family are highlighted in bold. Neighboring aromatic and basic residues in C-terminal part are given with orange and blue characters, respectively. c-d) Characteristic dynamics of TM dimers. Concerted motions in WT *R* (c) and V536E *r/l* (d) dimers delineated by the covariance analysis of 200 ns MD trajectories in POPC membrane. 2D maps of scalar products of Cα-atom projections of the first eigenvector (*left panels*) onto dimer conformations (*right panels*) representing the extremes of movements along the first eigenvector. Positive and negative values of scalar products depict, respectively, pairwise correlation and anticorrelation between directions of Ca-atoms displacement along the first eigenvector. Helices are shown in molecular surface representation, while green and red patches depict the position of V536 and E536, respectively. Cyan arrows depict the direction of movements. See also movies S1-S4 for visualization of the movements in the corresponding dimer conformations.

above analysis for the recently published MD simulations in the POPC bilayer (200 ns long) of the NMR-derived TM dimer conformations of EGFR [55] with the helices associated via their C– (non-active, b1C) and N-terminal regions (active, b1N) [15] [16] (Fig. S11a). The calculated concerted motions in b1N and b1C conformations show that these two states are prominently different in their characteristic dynamics (Fig. S11b). In the first case, a periodic intensity pattern corresponds to a rigid-body gear-like rotation of the helices (see also Fig. 5c, Movies S1, S2), while in the second case the only observed correlated motions correspond to the separation of the N-terminal regions. Importantly, in agreement with our all-atom simulations, the recent coarse-grained MD simulations of the EGFR TM dimer have shown how a combination of helix rotation and scissor-like motion (pivot) can shape the switch between active and non-active dimeric states [56].

4. Discussion

4.1. Contribution of TM dimerization to WT PDGFRA activation

In contrast to ErbB family receptors, the TM domain of WT PDGFRA lacks a well-defined polar (glycophorin-like) dimerization motifs (Fig. 1a). This suggests that the PDGFRA WT TM helices dimerize mostly through packing of aliphatic side-chains at the interface, which in turn results in multiple rotationally related states in the left- and right-handed Ω angle regions. Our analysis shows that such dimerization occurs via two distinct interfaces (I and II), with hybrid packing also possible (Fig. 3c). Moreover, our results show that the interface I

and II dimers differ in the characteristic dynamics of TM helices, which is responsible for allosteric signal transmission between the receptor's extracellular and kinase domains. Such ligand-induced symmetric or asymmetric rearrangements and scissoring of the TM helices required for downstream signal transmission have been detected recently in another class of membrane receptors - sensor histidine kinases [57]. In the case of PDGFRs, binding of two PDGF molecules to corresponding receptor sites leads to a dimerization of extracellular and TM regions of the receptors and an asymmetric dimerization of their kinase domains, as shown for PDGFRB using negative-stain electron microscopy imaging [22]. While the resolution in this experiment did not allow for a precise definition of the configuration of TM domains in the full-length ligand-bound PDGFRB dimer, the authors fitted the NMR structure of the PDGFRB left-handed TM dimer [21] to the electron density corresponding to the TM dimer and detergent molecules. This analysis has shown that in the activated receptor, the TM helices adopt an arrangement in which the N-termini remain close to each other. As we have demonstrated before, PDGFRA is able to form a dimer in the ligand-free state [6]. This, in turn, suggests that the TM dimer conformation present in the apo state likely rearranges in response to the mechanical input of ligand binding (Fig. 6).

According to MD data on EGFR, its active TM dimer (b1N) displays a specific dynamic mode characterized by a rotation of helices, which is absent in the non-active state (b1C, Fig. S11). The dynamic behavior of the b1N dimer, together with a higher level of lipid perturbation than

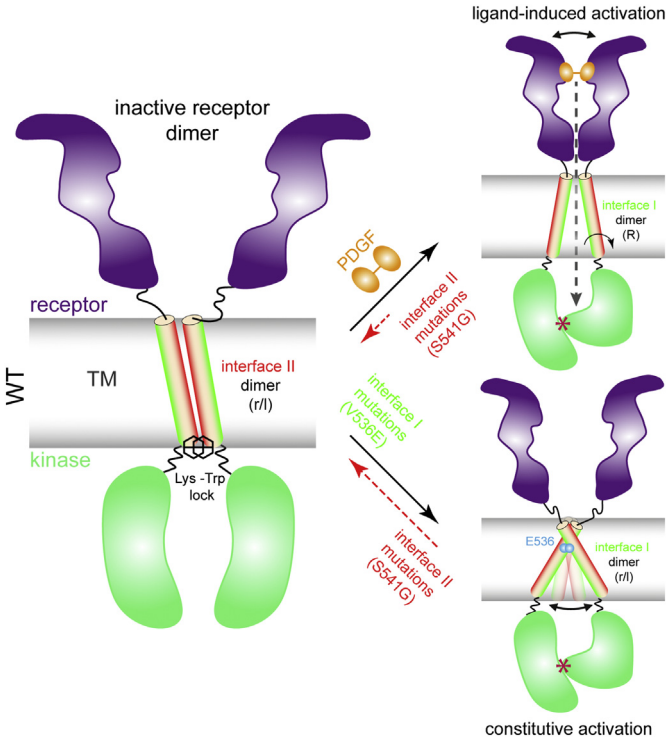

Fig. 6. Contribution of the TM domains to PDGFRA activation and its modulation by TM mutations. In WT ligand-free receptor dimer TM domains (cylinders) adopt near-parallel interface II (shown with red color) conformation, which locks the receptor in the inactive state. Binding of PDGF (yellow ovals) to the extracellular domains (violet blobs) pushes the TM dimer into the interface I (shown with green color) right-handed conformation, which transmits an allosteric signal to the downstream kinase domains (green blobs). Activating interface I mutations (V536E) allow spontaneous transitions between inactive interface II and active interface I TM dimers that may generate sufficient impulse to activate the kinase domains independently of the PDGF binding to the receptor. Interface II mutation S541G depletes "active" dimer conformations via stabilization of the "locked" interface II dimers that has dramatic effect for the constitutively active V536E.

for b1C [55], indicates that the former EGFR conformation may be metastable. This would diminish a spontaneous transition to the b1N state facilitating respective asymmetric association of kinase domains due to rotation of the helices and their arrangement into a transient asymmetric dimer. A comparison of MD data for the PDGFRA dimer conformations with the EGFR reference suggests that the PDGFRA WT interface I *R* dimer closely resembles the EGFR active dimer in geometric terms, but also when it comes to its dynamics and lipid interactions (Fig. 5c, Fig. S8, Fig. S11). In WT, spontaneous transition to *R* conformation is restricted by a significant free-energy penalty (Fig. 3a), where the dominant state of the dimer corresponds to the interface I *L* conformation and a switch to the *R* state also requires transition through the near-parallel *r/l* state with the interface II. Dimerization along the latter interface provides an arrangement, whereby W549 and K550 can form interacting cation-pi pairs (Fig. 5a). Indeed, the perturbation of NεH, NH W549 and NH K550 NMR signals upon dimerization of the WT TM domains (Fig. 4b) can be related to the interaction between these residues. We speculate that this "Lys-Trp lock", can provide an additional level of control of spontaneous activation, since it imposes physical constraints the displacement of C-termini (Fig. S5g, h). Such interactions between neighboring aromatic and basic residues could also shape activation via TM domains in other RTK members with similar sequence organization, such as in particular the RTK type III subfamily (Fig. 5b). Hence, in order to release the C-termini and give them sufficient freedom for rearrangements of the downstream kinase domains, the PDGFRA TM dimer should switch to the interface I conformation (Fig. 6). From this perspective, we cannot absolutely exclude the possibility that the WT *L* state (interface I) also facilitates the required arrangement for activation of the kinase domains. However, as this conformation typically corresponds to the low-energy states in ensembles of PDGFRA variants with negligible basal activity (WT, V536E/S541G) and as its dynamic modes lack a concerted rotation of the helices seen in the "genuine" active *R* conformation (or b1N dimer of EGFR), it probably corresponds to a partially active state, which would potentiate the low level of constitutive activation (Fig. 2). For example, such a state is found among rotationally related conformations of the TM dimer of thrombopoietin receptor [17]. Another possibility is that the left-handed interface I PDGFRA dimer, albeit energetically favorable and present in the PDGFRB TM dimer [21], represents a configuration, which is only formed by isolated TM domains, but not as a part of the full-length receptor.

4.2. Effect of TM mutations on the formation and dynamics of PDGFRA TM dimers

The association free energy of TM dimer conformations depends on direct protein-protein interactions, but also on the lipid environment [10] [35] [58]. Thus, *L* and *R* WT dimer conformations with the same interface, but different geometry, display different lipid perturbation effects (Fig. S8). According to both modeling and NMR data, the WT TM dimer ensemble is characterized by a single dominant state (Fig. 3a, Fig. 4b). On the other hand, the V536E substitution at interface I results in a redundant ensemble of the mutant dimer, displaying strong self-association in micellar environment (Fig. 4c, Fig. S4a). Namely, this mutation leads to an equilibrium, between active (interface I) and non-active (interface II) TM dimeric states (Fig. 3a) and thus facilitates spontaneous transitions between them and subsequent receptor activation (Fig. 2, Fig. 6). In addition, the Glu mutation also affects dynamics of individual states. For instance, the gear-like rotation of WT helices (Movie S1, S2) is not detected in conformations with a mutated interface I (*r/l* and *L*). In the WT, the aliphatic TM residues (representing "gear-teeth") are only able to form "transient" van-der-Waals contacts with the neighbors. On the other hand, polar Glu residues at the interface can form more stable electrostatic contacts (particularly, hydrogen bonds) with each other and the neighboring residues (Fig. S6), thus making the interface I more "sticky". Therefore,

the V536E mutation constrains the TM dimer and introduces a mechanical hinge in the middle of the dimer that changes its dynamic mode into scissor-like movement (Movies S3, S4). The latter mode enables easy transitions between mutually similar *L* and *r/l* states of the mutant dimer (Fig. S5). This, in turn, could generate a sufficient impulse to enable an active arrangement of kinase domains independently of PDGF binding (Fig. 6). Interestingly, the levels of spontaneous and ligand-induced activation are indistinguishable for the most constitutively active variants (Fig. 2): either the redundancy of the TM dimer ensemble potentiates both spontaneous activation and transitions within the ligand-bound receptor, or activation of the mutant always occurs independently of the rearrangements of extracellular domains. The latter possibility is supported by the fact that the S541G mutation at interface leads to stronger inactivation effect in V536E background as compared to WT and another constitutively active variant D842V, in which spontaneous activation does not rely on modulation of TM dimerization (Fig. S2). While the V536E/S541G functional phenotype is similar to that of WT according to functional assays (Fig. 2), the ensembles of TM dimer conformations of the two are rather different according to both modeling and NMR (Fig. 3b, Fig. S4). Thus, introduction of Gly at the interface II stabilize a dominant left-handed state with contacts in this region, while no favorable right-handed states for the double mutant could be identified. We observe a similar effect for other modeled Gly-mutants (L534G, I537G), where association becomes favorable for the mutated interface (Fig. 3). A lack of right-handed states of V536E/S541G with interface I dimerization indicates that they become too unstable, and can hardly form spontaneously. This could also explain a prominent reduction in both ligand-induced and constitutive activation of V536E/S541G as compared to both WT (Fig. 2b) and its less active S541G variant (Fig. S2). Note that the S541G mutation reducing WT activity also affects only interface II dimer conformation (Fig. S2), where it enables tighter contacts between helices. This results in shorter distances between the C-termini, thus enabling stronger interaction between W549 and Lys550. Interestingly, the WT *r/l* dimer converges to a similar conformation in our simulations as the dominant left-handed state of V536E/S541G, with a backbone RMSD of 0.23 nm (Fig. S7c). At the same time, V536E/S541G and the WT differ prominently in their oligomerization ability (Fig. S4). While WT is not prone to oligomerization, introduction of the polar Glu mutation in the middle of the TM region potentiates the formation of oligomeric states (Fig. S4b). There, the lipid environment forces the helices to form additional complexes in order to shield the entropically unfavorable interactions with the exposed Glu as in the V536E *R* state or the V536E/S541G dominant *L* state (Fig. S8, Fig. S7c). The tendency of the WT to avoid oligomerization, which differs from the mutants with a polar Glu in the middle of the TM helix, may partially explain why PDGFRA receptor is not targeted by the E5 papillomavirus oncogenic protein, as is known for its homolog PGDFRB. The key difference of the TM domains of these two receptors is the presence of an additional polar residue T545 in PDGFRB (near the position 536 in PDGFRA, Fig. 1a), which is important for the interactions of E5 with the preformed TM dimer [59]. Recently, different oligomeric TM states (tetramers, hexamers) have also been proposed for the PDGFRB/E5 heterocomplex [60]. Moreover, formation of oligomers of a higher order than dimers, which we observe in vitro for PDGFRA TM fragments containing the V536E substitution, may represent an important phenomenon with potentially direct implication for the abnormal constitutive activation of the mutant receptor. The latter requires further investigation and validation in vivo.

Altogether, the effect of TM mutations in PDGFRA results from an interplay between the chemical nature of mutations in question and their position. However, since TM dimers correspond to ensembles of conformations, the exact effect of mutations is difficult to predict without analyzing representative conformations. Glu screening illustrates this idea well. While interface II mutations exhibit an expected neutral effect, only one out of 5 interface I mutations, V536E, results in real activation and V533E give some intermediate effect (Fig. S1). Here, we should mention that at the interface I position 537, only Asp displays an activation effect, while Glu and Gly, which both should provide a strong perturbation as compared to native Ile, do not. Moreover, mutagenesis data indicates that TM sequence of PDGFRA is quite robust to perturbations of the normal receptor activation by random substitutions. At the same time, our simple strategy to scan for mutations using MUTSCORE calculations displays a good agreement with the experiment. While this straightforward approach requires further improvements to make it fully quantitative and capable of accounting for factors other than TM dimer ensemble redundancy, it does provide a rational framework for designing TM mutations if no structural information is available and, especially, if some reference mutations are already known.

5. Conclusion

Our analysis suggests that the structural and dynamic organization of the PDGFRA TM dimer ensembles is crucial for a spontaneous switch between active and non-active receptor states. However, it is difficult to conclude the same for ligand-induced activation since none of the tested mutations turn the receptor completely off, although they still induce dramatic changes in the dimerization of TM domains. Therefore, we speculate that in the normally functioning receptor the TM dimer represents a rather passive channel for allosteric signal transmission, while in the constitutively active receptor it assumes a more active role. Further modeling and biophysical studies of allosteric signal propagation in the full-length receptor should clarify this possibility. Importantly, the strong tendency of the oncogenic V536E mutant to oligomerize suggests a way to design a potential modulator for eliminating or reducing the level of pathological activity of the receptor via direct interaction with its TM domains. For design of such a modulators, we would consider the V536E *R* dimer conformation as a potential target. The arrangement of TM helices in this conformation allows for a formation of tetrameric structures, where additional TM helices can associate with the preformed dimer via the mutated interface I (Fig. S4b). If the latter interactions can stabilize the inactive dimer state, this would potentially lead to switching-off of the pathogenically active receptor. Thus, the most obvious candidate for modulating the V536E mutant receptor can just be its isolated TM helix. Albeit in a reverse manner, such a strategy would resemble the mechanism of activation of PDGFRB receptor by its TM domain interactions with papilloma virus E5 oncoprotein, an exogenous modulator optimized by natural selection.

Supplementary data to this article can be found online at https://doi.org/10.1016/j.bbagen.2018.09.011.

Acknowledgments

This work was supported by the Russian Science Foundation (grant 18-14-00375): MUTSCORE development, free-energy calcualtions and data analysis. Computational analysis of the membrane response effects was supported by the Russian Foundation for Basic Research: grants 16-04-00578 and 18-54-15007. NMR experiments were carried out in the framework of the Russian Foundation for Basic Research grant 18-04-01289. POPC simulations were supported by the European Research Council (Starting Independent grant 279408 to BZ). Authors are grateful to the “Molecular and Cellular Biology” RAS program. Supercomputer calculations were sponsored in the framework of the Basic Research Program at the National Research University Higher School of Economics (HSE) and the Russian Academic Excellence Project ‘5-100’. Access to computational facilities of the Supercomputer Center “Polytechnical” at the St. Petersburg Polytechnic University is greatly appreciated.

References

[1] F. Cymer, D. Schneider, Transmembrane helix-helix interactions involved in ErbB receptor signaling, Cell Adhes. Migr. 4 (2010) 299–312.
[2] K. Bugge, K. Lindorff-Larsen, B.B. Kragelund, Understanding single-pass transmembrane receptor signaling from a structural viewpoint-what are we missing? FEBS J. 283 (2016) 4424–4451.
[3] J. Andrae, R. Gallini, C. Betsholtz, Role of platelet-derived growth factors in physiology and medicine, Genes Dev. 22 (2008) 1276–1312.
[4] J.B. Demoulin, A. Essaghir, PDGF receptor signaling networks in normal and cancer cells, Cytokine Growth Factor Rev. 25 (2014) 273–283.
[5] F. Toffalini, J.B. Demoulin, New insights into the mechanisms of hematopoietic cell transformation by activated receptor tyrosine kinases, Blood 116 (2010) 2429–2437.
[6] A.I. Velghe, S. Van Cauwenberghe, A.A. Polyansky, D. Chand, C.P. Montano-Almendras, S. Charni, B. Hallberg, A. Essaghir, J.B. Demoulin, PDGFRA alterations in cancer: characterization of a gain-of-function V536E transmembrane mutant as well as loss-of-function and passenger mutations, Oncogene 33 (2014) 2568–2576.
[7] R.G. Verhaak, K.A. Hoadley, E. Purdom, V. Wang, Y. Qi, M.D. Wilkerson, C.R. Miller, L. Ding, T. Golub, J.P. Mesirov, G. Alexe, M. Lawrence, M. O'Kelly, P. Tamayo, B.A. Weir, S. Gabriel, W. Winckler, S. Gupta, L. Jakkula, H.S. Feiler, J.G. Hodgson, C.D. James, J.N. Sarkaria, C. Brennan, A. Kahn, P.T. Spellman, R.K. Wilson, T.P. Speed, J.W. Gray, M. Meyerson, G. Getz, C.M. Perou, D.N. Hayes, N. Cancer Genome Atlas Research, Integrated genomic analysis identifies clinically relevant subtypes of glioblastoma characterized by abnormalities in PDGFRA, IDH1, EGFR, and NF1, Cancer Cell 17 (2010) 98–110.
[8] A. Alentorn, Y. Marie, C. Carpentier, B. Boisselier, M. Giry, M. Labussiere, K. Mokhtari, K. Hoang-Xuan, M. Sanson, J.Y. Delattre, A. Idbaih, Prevalence, clinico-pathological value, and co-occurrence of PDGFRA abnormalities in diffuse gliomas, Neuro-Oncology 14 (2012) 1393–1403.
[9] A.H. Shim, H. Liu, P.J. Focia, X. Chen, P.C. Lin, X. He, Structures of a platelet-derived growth factor/propeptide complex and a platelet-derived growth factor/receptor complex, Proc. Natl. Acad. Sci. U. S. A. 107 (2010) 11307–11312.
[10] A.A. Polyansky, P.E. Volynsky, R.G. Efremov, Multistate organization of transmembrane helical protein dimers governed by the host membrane, J. Am. Chem. Soc. 134 (2012) 14390–14400.
[11] P.E. Volynsky, A.A. Polyansky, G.N. Fakhrutdinova, E.V. Bocharov, R.G. Efremov, Role of dimerization efficiency of transmembrane domains in activation of fibroblast growth factor receptor 3, J. Am. Chem. Soc. 135 (2013) 8105–8108.
[12] S.J. Fleishman, J. Schlessinger, N. Ben-Tal, A putative molecular-activation switch in the transmembrane domain of erbB2, Proc. Natl. Acad. Sci. U. S. A. 99 (2002) 15937–15940.
[13] E.V. Bocharov, K.S. Mineev, P.E. Volynsky, Y.S. Ermolyuk, E.N. Tkach, A.G. Sobol, V.V. Chupin, M.P. Kirpichnikov, R.G. Efremov, A.S. Arseniev, Spatial structure of the dimeric transmembrane domain of the growth factor receptor ErbB2 presumably corresponding to the receptor active state, J. Biol. Chem. 283 (2008) 6950–6956.
[14] P.E. Bragin, K.S. Mineev, O.V. Bocharova, P.E. Volynsky, E.V. Bocharov, A.S. Arseniev, HER2 Transmembrane Domain Dimerization coupled with Self-Association of Membrane-Embedded Cytoplasmic Juxtamembrane Regions, J. Mol. Biol. 428 (2016) 52–61.
[15] N.F. Endres, R. Das, A.W. Smith, A. Arkhipov, E. Kovacs, Y. Huang, J.G. Pelton, Y. Shan, D.E. Shaw, D.E. Wemmer, J.T. Groves, J. Kuriyan, Conformational coupling across the plasma membrane in activation of the EGF receptor, Cell 152 (2013) 543–556.
[16] E.V. Bocharov, D.M. Lesovoy, K.V. Pavlov, Y.E. Pustovalova, O.V. Bocharova, A.S. Arseniev, Alternative packing of EGFR transmembrane domain suggests that protein-lipid interactions underlie signal conduction across membrane, Biochim. Biophys. Acta 1858 (2016) 1254–1261.
[17] E.E. Matthews, D. Thevenin, J.M. Rogers, L. Gotow, P.D. Lira, L.A. Reiter, W.H. Brissette, D.M. Engelman, Thrombopoietin receptor activation: transmembrane helix dimerization, rotation, and allosteric modulation, FASEB J. 25 (2011) 2234–2244.
[18] E. Leroy, J.P. Defour, T. Sato, S. Dass, V. Gryshkova, M.M. Shwe, J. Staerk, S.N. Constantinescu, S.O. Smith, His499 Regulates Dimerization and Prevents Oncogenic Activation by Asparagine Mutations of the Human Thrombopoietin Receptor, J. Biol. Chem. 291 (2016) 2974–2987.
[19] A.J. Brooks, W. Dai, M.L. O'Mara, D. Abankwa, Y. Chhabra, R.A. Pelekanos, O. Gardon, K.A. Tunny, K.M. Blucher, C.J. Morton, M.W. Parker, E. Sierecki, Y. Gambin, G.A. Gomez, K. Alexandrov, I.A. Wilson, M. Doxastakis, A.E. Mark, M.J. Waters, Mechanism of activation of protein kinase JAK2 by the growth hormone receptor, Science 344 (2014) 1249783.
[20] E.V. Bocharov, D.M. Lesovoy, O.V. Bocharova, A.S. Urban, K.V. Pavlov, P.E. Volynsky, R.G. Efremov, A.S. Arseniev, Structural basis of the signal transduction via transmembrane domain of the human growth hormone receptor, Biochim. Biophys. Acta 1862 (2018) 1410–1420.
[21] C. Muhle-Goll, S. Hoffmann, S. Afonin, S.L. Grage, A.A. Polyansky, D. Windisch, M. Zeitler, J. Burck, A.S. Ulrich, Hydrophobic matching controls the tilt and stability of the dimeric platelet-derived growth factor receptor (PDGFR) beta transmembrane segment, J. Biol. Chem. 287 (2012) 26178–26186.
[22] P.H. Chen, V. Unger, X. He, Structure of Full-Length Human PDGFRbeta Bound to its Activating Ligand PDGF-B as Determined by Negative-Stain Electron Microscopy, J. Mol. Biol. 427 (2015) 3921–3934.
[23] A.A. Polyansky, A.O. Chugunov, P.E. Volynsky, N.A. Krylov, D.E. Nolde, R.G. Efremov, PREDDIMER: a web server for prediction of transmembrane helical dimers, Bioinformatics 30 (2014) 889–890.
[24] S. Pronk, S. Pall, R. Schulz, P. Larsson, P. Bjelkmar, R. Apostolov, M.R. Shirts, J.C. Smith, P.M. Kasson, D. van der Spoel, B. Hess, E. Lindahl, GROMACS 4.5: a high-throughput and highly parallel open source molecular simulation toolkit, Bioinformatics 29 (2013) 845–854.
[25] H.J.C. Berendsen, J.P.M. Postma, W.F. van Gunsteren, J. Hermans, Interaction models for water in relation to protein hydration, Place Published (1981).
[26] G. Bussi, D. Donadio, M. Parrinello, Canonical sampling through velocity rescaling, J. Chem. Phys. 126 (2007) 014101.
[27] H.J.C. Berendsen, J.P.M. Postma, W.F. van Gunsteren, A. Dinola, J.R. Haak, Molecular dynamics with coupling to an external bath, J. Chem. Phys. 81 (1984) 3684.
[28] B. Hess, H. Bekker, H.J.C. Berendsen, J.G.E.M. Fraaije, LINCS: a linear constraint solver for molecular simulations, J. Comput. Chem. 18 (1997) 1463–1472.
[29] J. Henin, A. Pohorille, C. Chipot, Insights into the recognition and association of transmembrane alpha-helices. The free energy of alpha-helix dimerization in glycophorin a, J. Am. Chem. Soc. 127 (2005) 8478–8484.
[30] K. Lindorff-Larsen, S. Piana, K. Palmo, P. Maragakis, J.L. Klepeis, R.O. Dror, D.E. Shaw, Improved side-chain torsion potentials for the Amber ff99SB protein force field, Proteins 78 (2010) 1950–1958.
[31] J.P. Jambeck, A.P. Lyubartsev, Derivation and systematic validation of a refined all-atom force field for phosphatidylcholine lipids, J. Phys. Chem. B 116 (2012) 3164–3179.
[32] W.L. Jorgensen, Quantum and Statistical Mechanical Studies of Liquids. 10. Transferable Intermolecular potential Functions for Water, Alcohols, and Ethers - Application to Liquid Water, J. Am. Chem. Soc. 103 (1981) 335–340.
[33] W.G. Hoover, Canonical dynamics: Equilibrium phase-space distributions, Phys. Rev. A Gen. Phys. 31 (1985) 1695–1697.
[34] M. Parrinello, A. Rahman, Polymorphic Transitions in Single-Crystals - a New Molecular-Dynamics Method, J. Appl. Phys. 52 (1981) 7182–7190.
[35] A.S. Kuznetsov, A.A. Polyansky, M. Fleck, P.E. Volynsky, R.G. Efremov, Adaptable Lipid Matrix Promotes Protein-Protein Association in Membranes, J. Chem. Theory Comput. 11 (2015) 4415–4426.
[36] L.L.C. Schrodinger, The PyMOL Molecular Graphics System, Version 1.3r1, (2010).
[37] F.A. Arts, D. Chand, C. Pecquet, A.I. Velghe, S. Constantinescu, B. Hallberg, J.B. Demoulin, PDGFRB mutants found in patients with familial infantile myofibromatosis or overgrowth syndrome are oncogenic and sensitive to imatinib, Oncogene 35 (2016) 3239–3248.
[38] F.W. Studier, Protein production by auto-induction in high density shaking cultures, Protein Expr. Purif. 41 (2005) 207–234.
[39] Y.K. Reshetnyak, O.A. Andreev, M. Segala, V.S. Markin, D.M. Engelman, Energetics of peptide (pHLIP) binding to and folding across a lipid bilayer membrane, Proc. Natl. Acad. Sci. U. S. A. 105 (2008) 15340–15345.
[40] J. Cavanagh, W.J. Fairbrother, A.G. Palmer, M. Rance, N.J. Skelton, Protein NMR Spectroscopy: Principles and Practice, 2nd Edition, (2007), pp. 1–888.
[41] E.V. Bocharov, D.M. Lesovoy, S.A. Goncharuk, M.V. Goncharuk, K. Hristova, A.S. Arseniev, Structure of FGFR3 transmembrane domain dimer: implications for signaling and human pathologies, Structure 21 (2013) 2087–2093.
[42] G.A. Vidal, D.E. Clark, L. Marrero, F.E. Jones, A constitutively active ERBB4/HER4 allele with enhanced transcriptional coactivation and cell-killing activities, Oncogene 26 (2007) 462–466.
[43] H. Yamamoto, K. Higasa, M. Sakaguchi, K. Shien, J. Soh, K. Ichimura, M. Furukawa, S. Hashida, K. Tsukuda, N. Takigawa, K. Matsuo, K. Kiura, S. Miyoshi, F. Matsuda, S. Toyooka, Novel germline mutation in the transmembrane domain of HER2 in familial lung adenocarcinomas, J. Natl. Cancer Inst. 106 (2014) djt338.
[44] S.I. Ou, A.B. Schrock, E.V. Bocharov, S.J. Klempner, C.K. Haddad, G. Steinecker, M. Johnson, B.J. Gitlitz, J. Chung, P.V. Campregher, J.S. Ross, P.J. Stephens, V.A. Miller, J.H. Suh, S.M. Ali, V. Velcheti, HER2 Transmembrane Domain (TMD) Mutations (V659/G660) that Stabilize Homo- and Heterodimerization are rare oncogenic drivers in Lung adenocarcinoma that respond to afatinib, J. Thorac. Oncol. 12 (2017) 446–457.
[45] L.A. Noel, F.A. Arts, C.P. Montano-Almendras, L. Cox, O. Gielen, F. Toffalini, C.Y. Marbehant, J. Cools, J.B. Demoulin, The tyrosine phosphatase SHP2 is required for cell transformation by the receptor tyrosine kinase mutants FIP1L1-PDGFRalpha and PDGFRalpha D842V, Mol. Oncol. 8 (2014) 728–740.
[46] L. Zhang, A. Polyansky, M. Buck, Modeling transmembrane domain dimers/trimers of plexin receptors: implications for mechanisms of signal transmission across the membrane, PLoS ONE 10 (2015) e0121513.
[47] A.J. Beevers, A. Nash, M. Salazar-Cancino, D.J. Scott, R. Notman, A.M. Dixon, Effects of the oncogenic V(664)E mutation on membrane insertion, structure, and sequence-dependent interactions of the Neu transmembrane domain in micelles and model membranes: an integrated biophysical and simulation study, Biochemistry 51 (2012) 2558–2568.
[48] K.S. Mineev, S.V. Panova, O.V. Bocharova, E.V. Bocharov, A.S. Arseniev, The Membrane Mimetic Affects the Spatial Structure and Mobility of EGFR Transmembrane and Juxtamembrane Domains, Biochemistry 54 (2015) 6295–6298.
[49] A.A. Polyansky, P.E. Volynsky, A.S. Arseniev, R.G. Efremov, Adaptation of a membrane-active peptide to heterogeneous environment. I. Structural plasticity of the peptide, J. Phys. Chem. B 113 (2009) 1107–1119.
[50] B. Peter, A.A. Polyansky, S. Fanucchi, H.W. Dirr, A Lys-Trp cation-pi interaction mediates the dimerization and function of the chloride intracellular channel protein 1 transmembrane domain, Biochemistry 53 (2014) 57–67.
[51] G. Manning, D.B. Whyte, R. Martinez, T. Hunter, S. Sudarsanam, The protein kinase complement of the human genome, Science 298 (2002) 1912–1934.
[52] C.C. David, D.J. Jacobs, Principal component analysis: a method for determining

the essential dynamics of proteins, Methods Mol. Biol. 1084 (2014) 193–226.
[53] M. Zhernenkov, D. Bolmatov, D. Soloviov, K. Zhernenkov, B.P. Toperverg, A. Cunsolo, A. Bosak, Y.Q. Cai, Revealing the mechanism of passive transport in lipid bilayers via phonon-mediated nanometre-scale density fluctuations, Nat. Commun. 7 (2016) 11575.
[54] L. Zhang, A.J. Sodt, R.M. Venable, R.W. Pastor, M. Buck, Prediction, refinement, and persistency of transmembrane helix dimers in lipid bilayers using implicit and explicit solvent/lipid representations: microsecond molecular dynamics simulations of ErbB1/B2 and EphA1, Proteins 81 (2013) 365–376.
[55] E.V. Bocharov, P.E. Bragin, K.V. Pavlov, O.V. Bocharova, K.S. Mineev, A.A. Polyansky, P.E. Volynsky, R.G. Efremov, A.S. Arseniev, The Conformation of the Epidermal Growth factor Receptor Transmembrane Domain Dimer Dynamically Adapts to the Local Membrane Environment, Biochemistry 56 (2017) 1697–1705.
[56] M. Lelimousin, V. Limongelli, M.S. Sansom, Conformational changes in the epidermal growth factor receptor: Role of the transmembrane domain investigated by coarse-grained Metadynamics free energy calculations, J. Am. Chem. Soc. 138 (2016) 10611–10622.
[57] I. Gushchin, I. Melnikov, V. Polovinkin, A. Ishchenko, A. Yuzhakova, P. Buslaev, G. Bourenkov, S. Grudinin, E. Round, T. Balandin, V. Borshchevskiy, D. Willbold, G. Leonard, G. Buldt, A. Popov, V. Gordeliy, Mechanism of transmembrane signaling by sensor histidine kinases, Science 356 (2017).
[58] F. Cymer, A. Veerappan, D. Schneider, Transmembrane helix-helix interactions are modulated by the sequence context and by lipid bilayer properties, Biochim. Biophys. Acta 1818 (2012) 963–973.
[59] D. Windisch, C. Ziegler, S.L. Grage, J. Burck, M. Zeitler, P.L. Gor'kov, A.S. Ulrich, Hydrophobic Mismatch Drives the Interaction of E5 with the Transmembrane Segment of PDGF Receptor, Biophys. J. 109 (2015) 737–749.
[60] A.G. Karabadzhak, L.M. Petti, F.N. Barrera, A.P.B. Edwards, A. Moya-Rodriguez, Y.S. Polikanov, J.A. Freites, D.J. Tobias, D.M. Engelman, D. Dimaio, Two transmembrane dimers of the bovine papillomavirus E5 oncoprotein clamp the PDGF beta receptor in an active dimeric conformation, Proc. Natl. Acad. Sci. U. S. A. 114 (2017) E7262–E7271.